Submitted for the proceedings of the Sentinel-3 for Science Workshop
held in Venice-Lido, Italy, 2-5 June 2015, ESA Special Publication SP-734

ASSESSMENT OF SENTINEL-3/OLCI SUB-PIXEL VARIABILITY AND PLATFORM IMPACT USING LANDSAT-8/OLI

Quinten Vanhellemont[(1)], Kevin Ruddick[(1)]

[(1)] Royal Belgian Institute of Natural Sciences (RBINS), Operational DirectorateNatural Environment, Gulledelle 100, 1200 Brussels E-mail: quinten.vanhellemont@naturalsciences.be

ABSTRACT

Validation and calibration of ocean colour sensors with in situ data is key for successful exploitation of their data. Ship campaigns are expensive and provide a low number of good matchups, whereas autonomous systems can typically provide a matchup for each cloud-free scene. With the distribution of free and high quality imagery from Landsat-8, the amount of natural spatial variability in the coastal zone becomes quantifiable, and the possible impact of measurement platforms (ships, moorings, structures) on the signal measured by the satellite becomes clear. Here we present the use of Landsat-8/OLI imagery (30m) to assess the spatial variability within a Sentinel-3/OLCI pixel (300m) at validation sites, as well as an illustration of the impacts of the measurement platforms on the satellite measurement.

1. INTRODUCTION

The calibration and validation of moderate resolution (250m+) optical sensors and their atmospheric correction algorithms remains a key issue for exploitation of ocean colour remote sensing data. Ship-borne campaigns are very useful for collecting in situ measurements of mass concentrations of suspended sediments, turbidity, chlorophyll concentration and apparent and inherent optical properties. Concerning satellite validation, they are typically not cost effective due to the low number of matchups with cloud- and glint-free satellite pixels. Autonomously measuring stations can drastically increase the number of good matchups with imagery from multiple optical satellite missions, typically giving a matchup per cloud free scene, or hundreds over the satellite's lifetime. These stations can measure above-water radiance, such as the AERONET-OC network [1], or turbidity and PAR attenuation below the water surface, such as the CEFAS Smartbuoys [2]. Moreover, by collecting long time-series of measurements at the same location they allow for a good characterisation of the validation site in terms of temporal (daily and seasonal) variability. On high resolution imagery, e.g. from Landsat-8, both the structures where these autonomous platforms are located and the impact of those structures on the local marine signal are obvious, e.g. turbid tidal wakes observed in offshore wind farms [3] and at a turbid water AERONET-OC site [4]. In this study, using Landsat-8 imagery, we explore (1) the small-scale spatial variability (natural or human induced) at sub-moderate resolution scale, and (2) the impact of large sampling platforms on the signal measured by a moderate resolution sensor, here focusing on the 300 m full resolution mode of the Ocean and Land Colour Imager on Sentinel-3 (S3/OLCI).

2. METHODS

We use imagery from the Operational Land Imager on Landsat-8 (L8/OLI) of the Belgian coastal zone. OLI is an 8 band push-broom scanner with 7 bands at 30 m spatial resolution and 1 panchromatic band at 15 m resolution. Thanks to its excellent SWIR bands and, a greatly improved signal to noise ratio compared to previous Landsat imagers, OLI has proven to be very useful for coastal zone monitoring [3], [5]–[9]. For the assessment of spatial variability of turbidity - strongly correlated to mass concentration of suspended sediments - the L8/OLI imagery is atmospherically corrected according to [7]. Rayleigh reflectance is calculated based on sun and sensor geometry using 6SV [10]. The aerosol correction assumes a black SWIR (at 1.6 and 2.2 μm) over water [11] with a fixed aerosol model over the sub-scene. The aerosol reflectance is extrapolated from the 2.2 micron band using an exponential aerosol model.

Turbidity (~ side scattering at a NIR wavelength) is calculated using a switching turbidity algorithm [12]. Turbidity is calculated using the water leaving radiance reflectances in the 655 nm and the 865 nm channels on L8/OLI. The algorithm uses the same form as the algorithm by [13]:

$$T = \frac{A^{\lambda} \cdot \rho_w(\lambda)}{1 - \rho_w(\lambda) / C^{\lambda}} \quad (1)$$

with calibration coefficients A^{λ} = 228.1, 3078.9 (FNU) and C^{λ} = 0.1641, 0.2112 for λ = 655 and 865 nm respectively. Turbidity is derived solely from ρ_w 655 when ρ_w 655 < 0.05, and solely from ρ_w 865 when ρ_w 655 > 0.07. A linear blending is applied for ρ_w 655 between 0.05 and 0.07.

Imagery is resampled to OLCI (300 m) resolution, using the arithmetic mean average of 10x10 OLI 30 m pixels. The standard deviation and coefficient of variation (CV, standard deviation divided by the mean) are calculated per aggregated pixel. In order to assess platform impact, a target (platform) and a reference pixel are selected. Top of atmosphere reflectance (ρ_{TOA}) is extracted from a 10x10 pixel box (300 m) centred on the lower left corner of the target pixel. The 10x10 pixel box is averaged at TOA to represent the moderate resolution OLCI pixel. Then the Rayleigh and aerosol corrections [7] are applied for the moderate resolution pixel and the target and reference pixels.

3. RESULTS AND DISCUSSION

Figure 1 shows the high variability of surface suspended sediments in the Belgian coastal zone, both in spring (a, 2014-03-16) and at the end of summer (b, 2014-09-08). Long turbid wakes of the big container ships en route to Antwerpen can be seen in the main navigational channels. Turbidity for those scenes is shown in Figure 2, showing the high turbidity over the shallow sand banks in front of the coast and above the Vlakte van de Raan. Sediment transport into the port of Zeebrugge is observed during flood tide with the current going from west to east along the shore. A large difference between spring (some areas >100 NTU) and summer (generally <50 NTU) surface turbidity is observed, corresponding well to the seasonal trends observed with SeaWiFS, MODIS and MERIS [14].

The coefficient of variation (CV) is used to assess the sub-moderate-resolution pixel variability, here within a 300 m or 10x10 box of Landsat pixels, corresponding to Sentinel-3/OLCI resolution. The CV is remarkably stable within certain features in the image (around 5%), but shows high values (exceeding 30%) near short length scale features such as turbid wakes and fronts. There is a slight increase in the CV towards the offshore part of the image, because of the generally low signal at 655 nm in these clearer pixels. Pixel contamination of platforms and constructions (including their shadows) can be seen as high CV values at the offshore windfarms.

A subset over a small ship and its white foam wake from Figure 1a is shown in Figure 4. The ship clearly has a different reflectance spectrum than the surrounding water pixels (Figure 5a) and it and its wake impact the reflectance even at a 300 m aggregated pixel, especially in the NIR and SWIR (Figure 5b). In this case, the combined impact of the ship and its wake has a similar spectral shape as an aerosol and is for a large part corrected by the aerosol correction (Figure 5c). For larger ships, impacts similar to the platform (paragraph below) are found.

Figure 6 shows a subset of Figure 1b, over the CPower windfarm and the Offshore Transformer Station (OTS) where an Aeronet-OC station is now installed. The individual wind turbines and the OTS and their shadows on the water surface can be clearly discriminated at OLI resolution (30 m). The platform has quite a different spectral shape compared to the surrounding waters (Figure 7a), especially in the red-NIR-SWIR region. Figure 7b shows the reference pixel and the mean average of a 10x10 pixel box (300 m) centred on the lower left corner of the platform The large OTS platform also impacts this moderate resolution pixel, especially in the NIR and SWIR. A difference with the reference pixel is also found in the red band as a result of the red colour of the top of the platform. Due to the impact of the platform on the simulated moderate resolution pixel, the aerosol reflectance is overestimated in the aerosol correction (Figure 7c). Hence, the retrieved ρ_w is lower than the reference pixel and the atmospheric correction even fails in the NIR (ρ_w <0).

4. CONCLUSION

The Operational Land Imager on Landsat-8 (L8/OLI) is an excellent tool for coastal zone monitoring, especially in turbid waters. Its high spatial resolution (30 m) allows for the characterisation of spatial variability in coastal waters and around permanent validation sites. It also allows for the evaluation of new potential sites. Spatial variability is found to be quite stable even in very turbid waters, with the highest variability found at features with short spatial scales such as fronts and turbid wakes associated with constructions and ships. An archive of Landsat-8 imagery could be used to quantify typical spatial variability within moderate resolution pixels, and could aid selecting one-off or permanent validation sites. Even higher resolution data might be required in some cases (e.g. from Pléiades, 2.8 m) as significant spatial variability of surface suspended matter exists at <10 m scale.

As demonstrated here, for some validation sites moderate resolution (here taken as 300 m) pixels might be contaminated by the structure containing the in situ instruments. As the structures are typically much more reflective in the NIR and SWIR parts of the spectrum than the surrounding waters, the atmospheric correction will be impacted as it strongly relies on these longer wavelengths for the correction of aerosol scattering. For these structures it is strongly advised to characterize the area around the instrument using high resolution data and to identify an appropriate representative and uncontaminated reference or ‘twin’ pixel. For smaller ships with white foam wakes, the top of atmosphere signal is also impacted, but the difference looks like aerosol scattering, and is largely corrected in the atmospheric correction (cfr. [15]). Larger ships will contaminate the moderate resolution pixel to a larger

degree, and a different pixel might need to be selected for the match-up analysis.

The methodology described here is also applicable to the upcoming Multi Spectral Imager on Sentinel-2 (S2/MSI), which has a number of channels in the VIS-NIS at resolutions between 10 and 60 m, with a pair of SWIR bands at 1.6 and 2.2 µm for the atmospheric correction.

ACKNOWLEDGEMENTS

USGS/NASA is thanked for L8 data. Work was performed for the the European Community's Seventh Framework Programme (FP7/2007-2013) under grant agreement n° 606797 (HIGHROC project).

5. REFERENCES

[1] G. Zibordi, B. Holben, I. Slutsker, D. Giles, D. D'Alimonte, F. Mélin, J.-F. Berthon, D. Vandemark, H. Feng, G. Schuster, and others, "AERONET-OC: a network for the validation of ocean color primary products.," *J. Atmospheric Ocean. Technol.*, vol. 26, no. 8, 2009.

[2] D. K. Mills, R. W. P. M. Laane, J. M. Rees, M. Rutgers van der Loeff, J. M. Suylen, D. J. Pearce, D. B. Sivyer, C. Heins, K. Platt, and M. Rawlinson, "Smartbuoy: A marine environmental monitoring buoy with a difference," in *Elsevier Oceanography Series*, vol. 69, N. C. F., K. Nittis and S. E. Petersson H. Dahlin, Ed. Elsevier, 2003, pp. 311–316.

[3] Q. Vanhellemont and K. Ruddick, "Turbid wakes associated with offshore wind turbines observed with Landsat 8," *Remote Sens. Environ.*, vol. 145, pp. 105–115, 2014.

[4] Q. Vanhellemont, S. Bailey, B. Franz, and D. Shea, "Atmospheric Correction of Landsat-8 Imagery Using SeaDAS.," in *ESA Special Publication SP-726*, Frascati, 2014.

[5] B. A. Franz, S. W. Bailey, N. Kuring, and P. J. Werdell, "Ocean color measurements with the Operational Land Imager on Landsat-8: implementation and evaluation in SeaDAS," *J. Appl. Remote Sens.*, vol. 9, no. 1, pp. 096070–096070, 2015.

[6] D. Sun, C. Hu, Z. Qiu, and K. Shi, "Estimating phycocyanin pigment concentration in productive inland waters using Landsat measurements: A case study in Lake Dianchi," *Opt. Express*, vol. 23, no. 3, pp. 3055–3074, 2015.

[7] Q. Vanhellemont and K. Ruddick, "Advantages of high quality SWIR bands for ocean colour processing: examples from Landsat-8," *Remote Sens. Environ.*, vol. 161, pp. 89–106, 2015.

[8] Q. Vanhellemont and K. Ruddick, "Landsat-8 as a Precursor to Sentinel-2: Observations of Human Impacts in Coastal Waters.," in *ESA Special Publication SP-726*, Frascati, 2014.

[9] G. Wu, L. Cui, L. Liu, F. Chen, T. Fei, and Y. Liu, "Statistical model development and estimation of suspended particulate matter concentrations with Landsat 8 OLI images of Dongting Lake, China," *Int. J. Remote Sens.*, vol. 36, no. 1, pp. 343–360, 2015.

[10] E. Vermote, D. Tanré, J. Deuzé, M. Herman, J. Morcrette, and S. Kotchenova, "Second simulation of a satellite signal in the solar spectrum-vector (6SV)," *6S User Guide Version*, vol. 3, 2006.

[11] M. Wang, "Remote sensing of the ocean contributions from ultraviolet to near-infrared using the shortwave infrared bands: simulations," *Appl. Opt.*, vol. 46, no. 9, pp. 1535–1547, 2007.

[12] A. Dogliotti, K. Ruddick, B. Nechad, D. Doxaran, and E. Knaeps, "A single algorithm to retrieve turbidity from remotely-sensed data in all coastal and estuarine waters," *Remote Sens. Environ.*, vol. 156, pp. 157–168, 2015.

[13] B. Nechad, K. Ruddick, and G. Neukermans, "Calibration and validation of a generic multisensor algorithm for mapping of turbidity in coastal waters," in *SPIE Europe Remote Sensing*, 2009, p. 74730H–74730H.

[14] Q. Vanhellemont and K. Ruddick, "Generalized satellite image processing: eight years of ocean colour data for any region on earth," in *Proc. SPIE 8175, Remote Sensing of the Ocean, Sea Ice, Coastal Waters, and Large Water Regions 2011, 81750Q (October 07, 2011)*, 2011.

[15] H. R. Gordon and M. Wang, "Influence of oceanic whitecaps on atmospheric correction of ocean-color sensors," *Appl. Opt.*, vol. 33, no. 33, pp. 7754–7763, 1994.

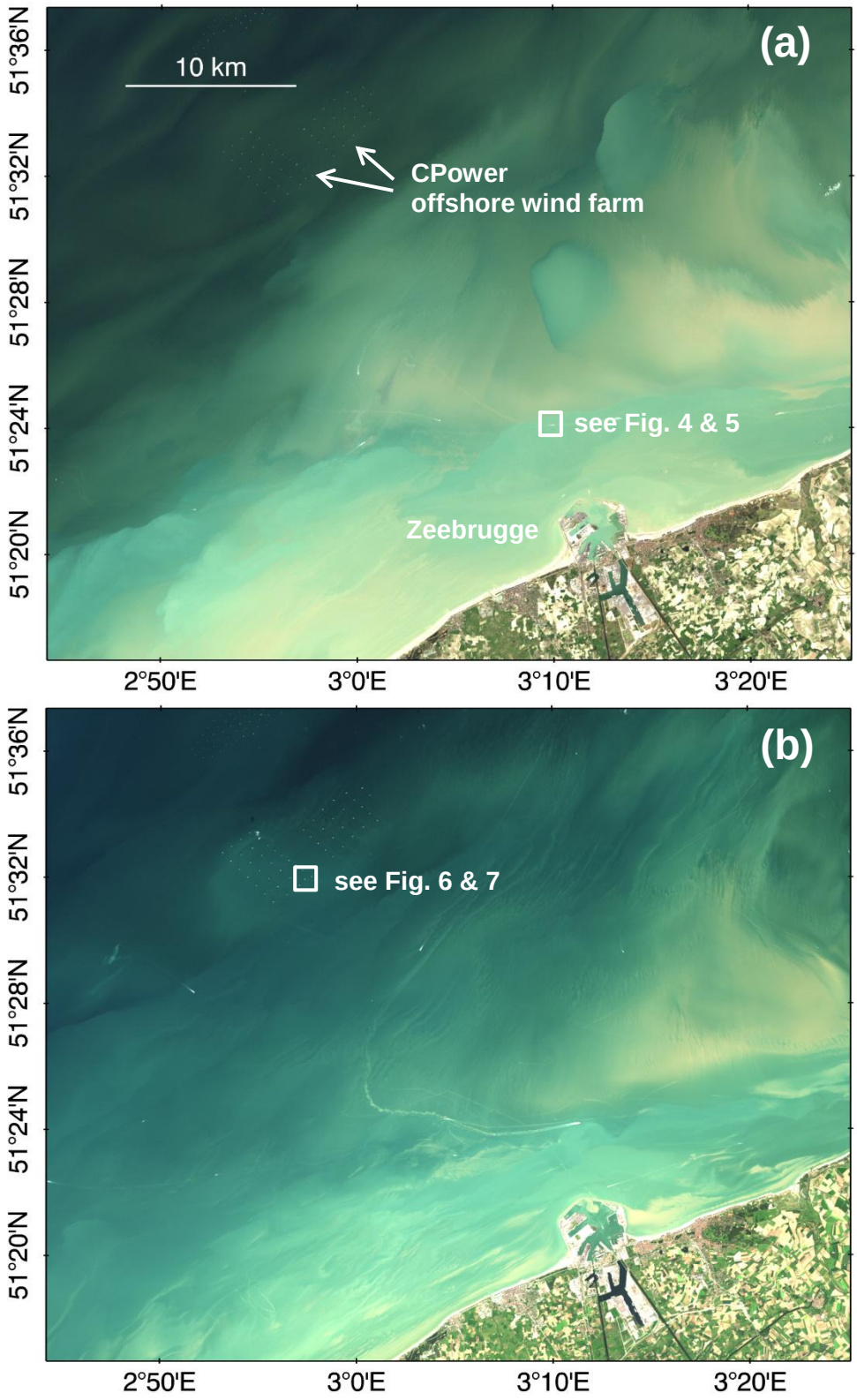

Figure 1 Rayleigh corrected Landsat-8 image (composite of channels 4,3,2) of the Belgian coastal zone on (a) 2014-03-16 (scene LC1990242014251LGN00) and (b) 2014-09-08 (scene LC1990242014251LGN00). High natural and human induced variability of suspended sediments can be observed. Subsets are shown in Figure 4 and Figure 6.

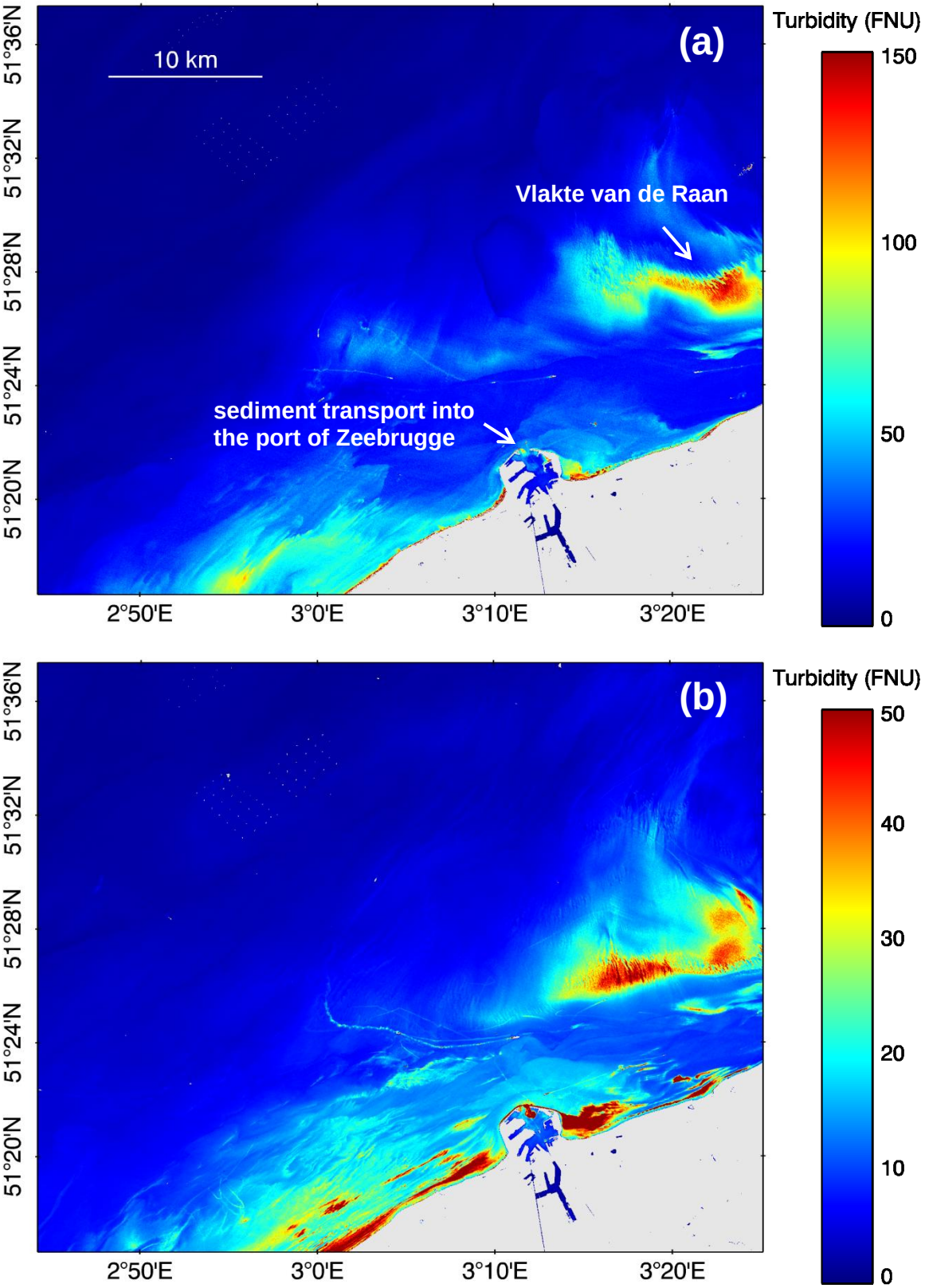

Figure 2 Turbidity derived from Landsat-8 (a) 2014-03-16 (scene LC1990242014251LGN00) and (b) 2014-09-08 (scene LC1990242014251LGN00) using Dogliotti et al. (2015). High turbidity is found over the shallow sandbanks near the coast, over the Vlakte van de Raan, in and around the port of Zeebrugge and in the wake of large container ships. Note the different colour scale for the spring (0-150 NTU) and summer (0-50 NTU) images.

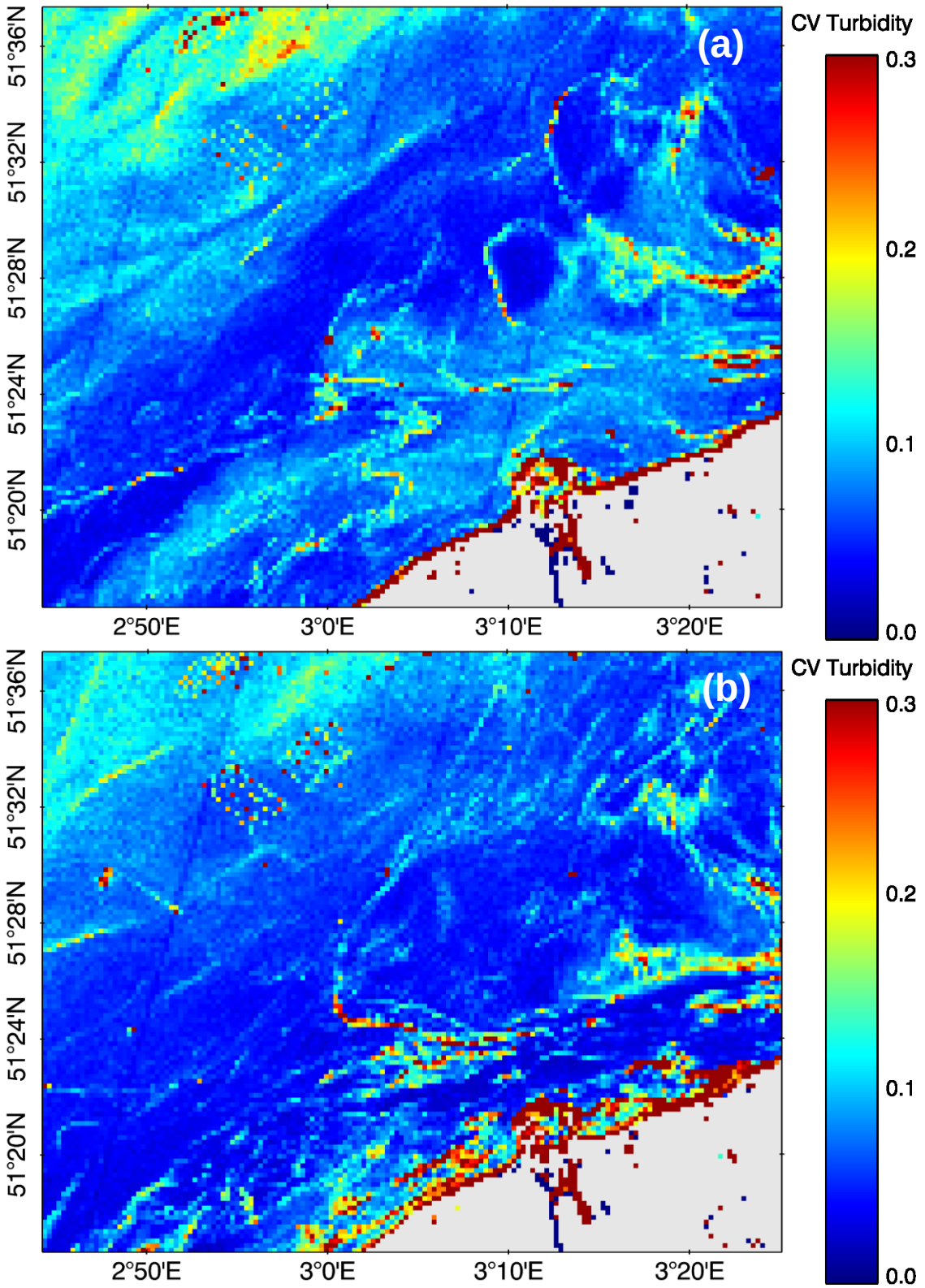

Figure 3 Spatial variability of turbidity (see Figure 2) expressed as the coefficient of variation, CV, (standard deviation divided by the mean) after aggregation of OLI 30m pixels to S3/OLCI 300m pixels (10x10). The highest CV is typically found near short length scale features such as fronts and turbid wakes of ships. The diagonal lines are the OLI detector boundaries.

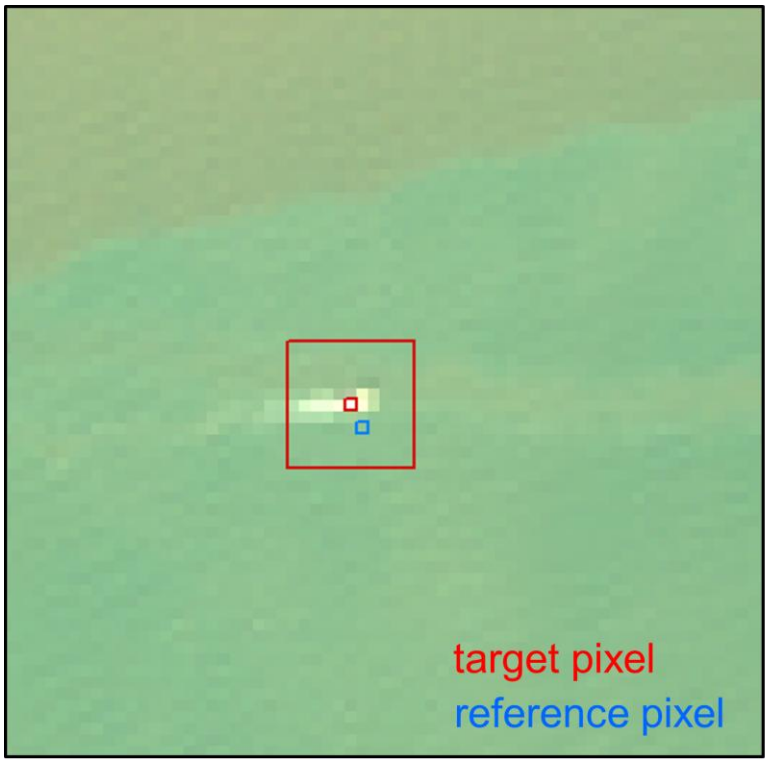

Figure 4 A subset of Figure 1a, showing a ship and its white foam wake in the Belgian coastal zone. The target pixel and box and the reference pixel are identified in red and blue respectively (see text for details).

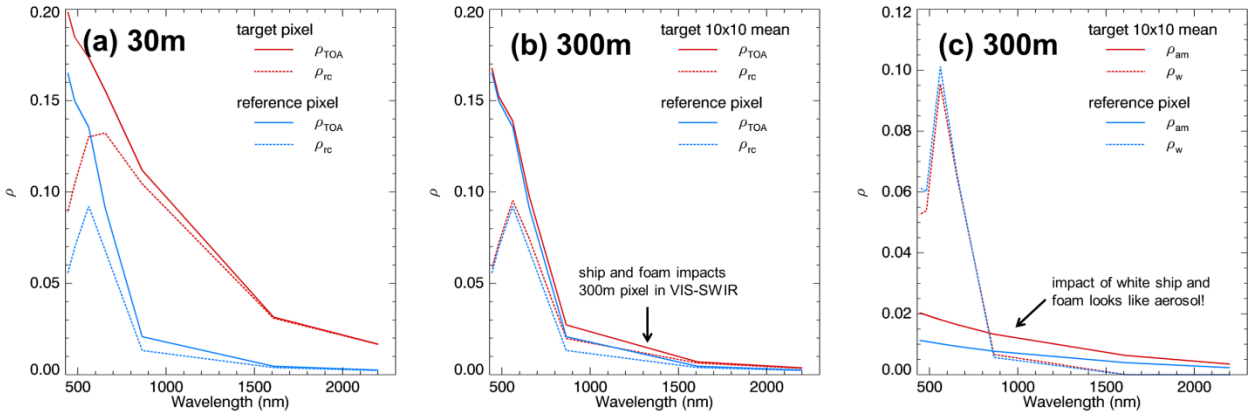

Figure 5 Top of atmosphere (ρ_{TOA}) and Rayleigh corrected (ρ_{rc}) spectra for a boat pixel (target pixel, red) and a reference pixel (blue) at OLI resolution (30 m) from scene LC1990242014075LGN00, (b) ρ_{TOA} and ρ_{rc} spectra for the arithmetic mean of a 10x10 pixel box containing the ship and its wake (red) and the reference pixel (blue) at OLI resolution (30 m), and (c) the water leaving radiance reflectance (ρ_w) and multiple-scattering aerosol reflectance (ρ_{am}) derived using [7] from the 10x10 pixel box average (red) and the reference pixel (blue).

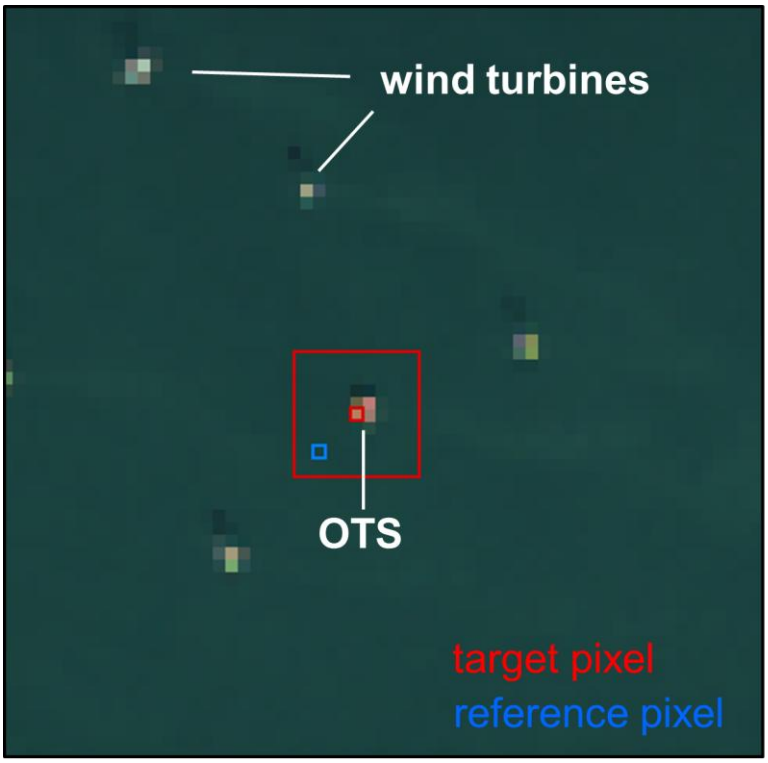

Figure 6 A subset of Figure 1b, showing a part of the C-Power wind farm, and the offshore transformer platform (OTS), where an Aeronet-OC station is installed. The target pixel and box and the reference pixel are identified in red and blue respectively (see text for details).

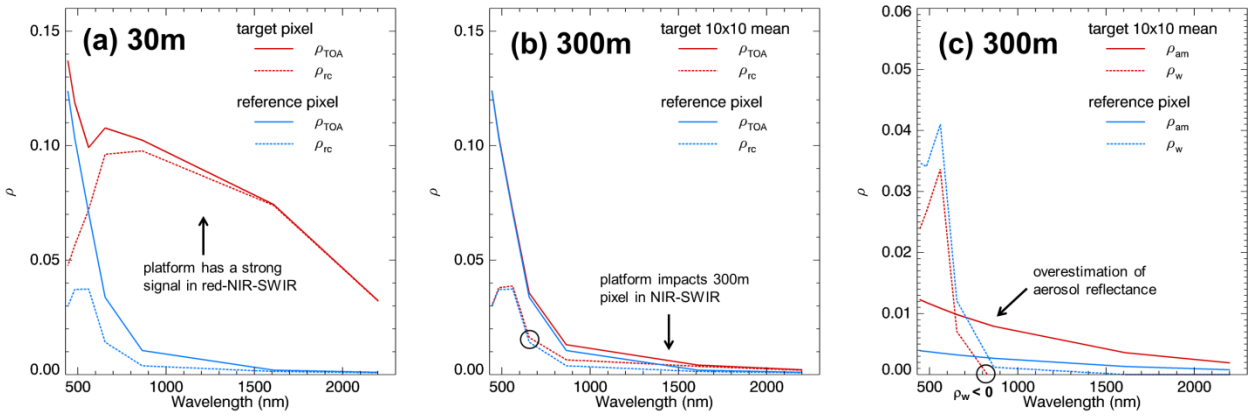

Figure 7 (a) Top of atmosphere (ρ_{TOA}) and Rayleigh corrected (ρ_{rc}) spectra for a platform pixel (target pixel, red) and a reference pixel (blue) at OLI resolution (30m) from scene LC1990242014251LGN00, (b) ρ_{TOA} and ρ_{rc} spectra for the arithmetic mean of a 10x10 pixel box containing the OTS platform (red) and the reference pixel (blue) at OLI resolution (30 m), and (c) the water leaving radiance reflectance (ρ_w) and multiple-scattering aerosol reflectance (ρ_{am}) derived using [7] from the 10x10 pixel box average (red) and the reference pixel (blue).